JOURNAL OF GEOPHYSICAL RESEARCH, VOL. 117, B01207, doi:10.1029/2011JB008769, 2012

Aerodynamics of stratovolcanoes during multiphase processes

Domenico M. Doronzo,[1,2] Joan Martí,[3] Roberto Sulpizio,[2,4] and Pierfrancesco Dellino[2]

Received 10 August 2011; revised 30 November 2011; accepted 5 December 2011; published 28 January 2012.

[1] Pyroclastic density currents (PDCs) are gas-particle flows generated during explosive eruptions, which are often erupted over the flanks of stratovolcanoes. These volcanoes may have different shapes, which can affect the flow aerodynamics and hence the depositional processes. Here, multiphase numerical simulations are carried out in order to define semiquantitative relationships among the PDC behavior, particle response, and deposit formation. Three stratovolcano shapes are used: straight, convex and concave, and, by means of numerical simulations, their effects both on the flow structure and depositional processes are highlighted. The current starts moving as a homogeneous flow, and then it rapidly evolves to a turbulent boundary layer moving in contact with the ground, overlaid by a companion wake region. Results show that thin boundary layers produce thick deposits of massive layers, whereas thick boundary layers produce thin laminated deposits. Moreover, concave wake regions would produce thick massive deposits of fine ash, whereas convex wake regions would produce thin ash deposits.

Citation: Doronzo, D. M., J. Martí, R. Sulpizio, and P. Dellino (2012), Aerodynamics of stratovolcanoes during multiphase processes, *J. Geophys. Res.*, *117*, B01207, doi:10.1029/2011JB008769.

1. Introduction

[2] A stratovolcano, also known as a composite volcano, is an imposing conical edifice built up by many layers of hardened lava, scoria, pumice, and ash [*Cas and Wright*, 1987]. Unlike shield volcanoes, stratovolcanoes are characterized by a steep profile and experience periodic explosive eruptions, which make them the most dangerous volcanoes in the world.

[3] Famous examples of straight- and concave-like composite volcanoes, at least for most of the profile, are Merapi (Indonesia) and Fuji (Japan), respectively, whereas some sectors of Teide (Canary Islands, Spain) are a rare example comparable to a convex-like volcano. Furthermore, subglacial shield volcanoes (e.g., Katla, Iceland) or other volcanoes mainly characterized by the propagation of lava flows (e.g., Etna, Italy) sometimes experience pyroclastic density current- (PDC-) forming explosive eruptions, so these volcanoes also fall within the category of composite volcanoes.

[4] The most hazardous event associated with explosive eruptions is the propagation of pyroclastic density currents (PDCs), which are gas-particle flows that move at high velocities down the volcano and over the surrounding topography [e.g., *Valentine and Fisher*, 1993; *Branney and Kokelaar*, 2002; *Sulpizio and Dellino*, 2008]. The physics of PDCs can be described in terms of a mixture of two components, represented by the solid particles and the fluid phase. This leads to the identification of a concentrate and a dilute end-member, in which transport and depositional processes are dominated by particle-particle interaction and by fluid turbulence, respectively [*Burgisser and Bergantz*, 2002].

[5] As a PDC moves over the volcano substrate, processes of deposition and erosion, as well as decoupling, blocking, or buoyancy of the flow, may occur in the flow-substrate interaction zone [*Valentine*, 1987; *Bursik and Woods*, 1996; *Branney and Kokelaar*, 2002; *Doronzo et al.*, 2010]. These processes depend on the morphologic conditions of the volcano (topography), which play an important role in the emplacement of the PDC deposits [*Branney and Kokelaar*, 2002; *Sulpizio and Dellino*, 2008].

[6] The sedimentological features of these deposits vary from massive to laminated facies, with a continuous or sharp transition in between [*Vazquez and Ort*, 2006; *Sulpizio et al.*, 2010], and each deposit represents the response of the particles to the fluid dynamic character of the flow in a specific time and space. The aerodynamic features of a stratovolcano, i.e., its shape point by point, thus strongly affect the local flow behavior, which means that the volcano could be regarded as a solid body immersed in a particle-laden fluid flow.

[7] Here, the influence of the shape of stratovolcanoes on fluid flow, as well as on particle transport and deposition, is investigated from the point of view of aerodynamics, which is a topic recently developed in multiphase volcanic currents [*Doronzo et al.*, 2010]. In particular, first a literature analysis on the development of a dilute PDC over a stratovolcano is carried out; then a computational analysis, allowing us to highlight the effects of the volcano shape on boundary layer processes, is performed. Finally, some general conclusions

[1]School of Earth and Atmospheric Sciences, Georgia Institute of Technology, Atlanta, Georgia, USA.
[2]Centro Interdipartimentale di Ricerca sul Rischio Sismico e Vulcanico, Dipartimento di Scienze della Terra e Geoambientali, Università degli Studi di Bari, Bari, Italy.
[3]Institute of Earth Sciences "Jaume Almera," CSIC, Barcelona, Spain.
[4]IDPA-CNR, Milan, Italy.

0148-0227/12/2011JB008769

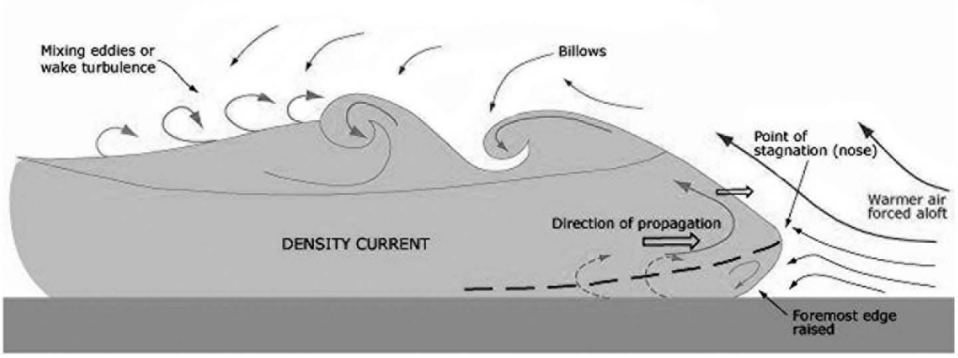

Figure 1. Scheme of a density current, such as a dilute pyroclastic density current, moving at contact with the substrate as the turbulent shear flow of fluid dynamics.

are drawn on the relationships between boundary layer conditions and emplacement of dilute PDC deposits.

[8] This paper uses as benchmark the paper of *Doronzo et al.* [2010], who have deduced the style of deposition from dilute PDCs through numerical simulations and calculated the sedimentation rate that occurs over the substrate as the currents interact with different topographies. That study was carried out from the point of view of particles, which means that the sediment flux toward the substrate was calculated from the simulations.

[9] Here, a parallel study is presented, but it is performed from the point of view of the continuous phase (gas), which means that the profiles of flow velocity are calculated from the simulations, and they are then related to the sediment flux of the discrete phase (particle). The aim of the paper is to highlight how the fluid flow acts on both the particle transport and deposition in a dynamical continuum (zero-velocity transport is deposition or final stop for a particle) in response to the volcano aerodynamics. In particular, the results of the simulations of *Valentine et al.* [2011] are postprocessed in light of the concept of aerodynamics of stratovolcanoes, and they are used to constrain the relationships between volcanic gas and particle behavior in PDCs.

2. Turbulent Boundary Layer on Stratovolcanoes

[10] PDCs can be generated during explosive eruptions because of both the vertical collapse of an eruptive column and the radial expansion of an overpressurized jet or dome explosion [e.g., *Wilson et al.*, 1980; *Branney and Kokelaar*, 2002; *Sulpizio and Dellino*, 2008; *Dellino et al.*, 2010a]. If they originate from the gravitational failure of a dome or part of the volcano edifice [e.g., *Lipman and Mullineaux*, 1981; *Esposti Ongaro et al.*, 2008], they propagate down a volcano as unidirectional flows. Small-volume PDCs generated from these mechanisms start developing from the collapse of the erupted gas-particle mixture, and they are driven by the shear stress on contact with the substrate, which is proportional to the dynamic pressure pulse of the collapsing mixture on impact with the ground. The case of large-volume ignimbrite-forming PDCs, in which the continuous feeding of the flow strongly influences the driving shear stress over time, is different [*Branney and Kokelaar*, 1992; *Martí et al.*, 2000].

[11] Numerical simulations and experiments of column collapse, as well as eyewitness reports of building collapse, reveal that the currents may be relatively concentrated in the impact zones [*Dellino et al.*, 2008; *Doronzo*, 2010] and the velocity may be roughly homogeneous with flow height [*Doronzo et al.*, 2011], which contributes forming PDC deposits with a massive facies [*Dellino et al.*, 2010b]. After the rapid collapse of the suspended particle load near the crater, the flows behave as the mixing layers of fluid dynamics, i.e., they are subject to the Kelvin-Helmholtz instability because of the sharp transition between the moving flows and the surrounding atmospheric air [*Dufek and Bergantz*, 2007]. Big vortices are thus generated on top of the flows because of the instability, which expands the PDCs as they increase in size (because of particle sedimentation and hence flow dilution) and are tilted upcurrent by frictional resistance effects of the air. At the same time, the no-slip condition (zero velocity) strongly affects the flows in contact with the ground by creating a steep velocity gradient (Figure 1).

[12] Such an evolution of dilute PDCs, as they travel from the impact zone to the far field, is ascribed to the classic development of the wall flows of fluid dynamics, which are characterized by a logarithmic velocity profile in the lower part of the flow with increasing upward velocity (turbulent boundary layer) and a cumulative Gaussian profile in the upper part with decreasing upward velocity (free-wall jet) [*Kneller et al.*, 1999; *Dellino et al.*, 2010b; *Doronzo et al.*, 2011]. Dilute PDCs are thus subject to a stratification of velocity, as well as density, in that the lower part is continuously fed by the particles that settle through the gas [*Valentine*, 1987; *Dellino et al.*, 2004]. In particular, at the base of the turbulent boundary layer there is a flow boundary zone, which is the zone fed by the upper particles of the lower flow where the sedimentary structures are acquired [*Branney and Kokelaar*, 2002].

[13] The boundary layer processes of sedimentation and deposition lead to the emplacement of PDC deposits with layered or laminated facies, whereas the wake region processes give fine-grained fall deposits with massive facies, which cap the flow deposits [e.g., *Sulpizio et al.*, 2007; *Dellino et al.*, 2010b]. In the case of lava dome explosions, PDCs are driven by the overpressure existing between the dome and the surrounding atmosphere, as well as by gravity, and they have the same evolution of column-collapse-generated PDCs, in which a homogeneous gas-particle mixture evolves to a turbulent boundary layer overlaid by a

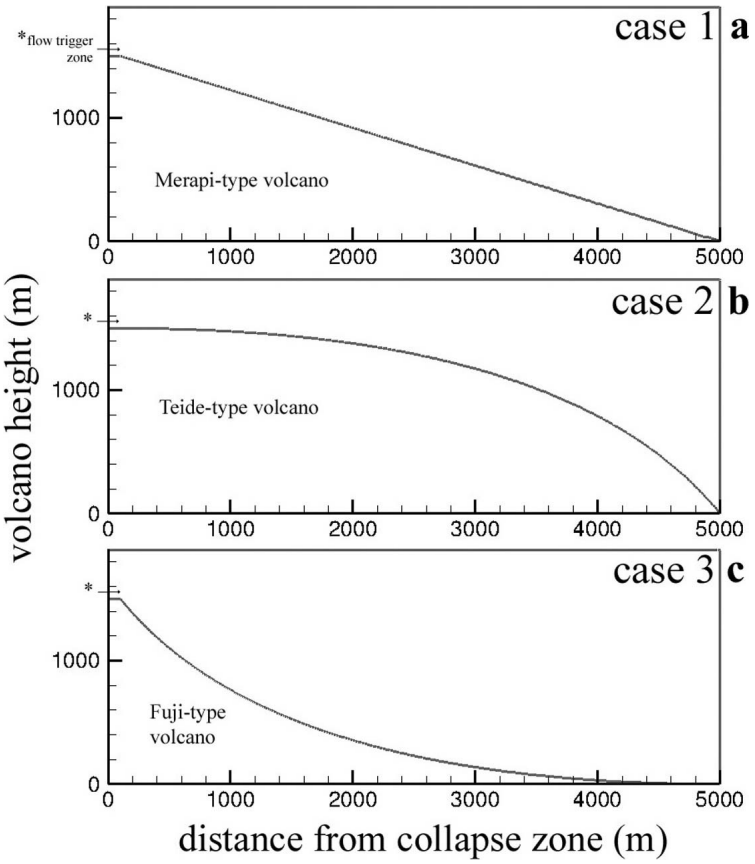

Figure 2. The three geometries used for simulating the shape of a stratovolcano. (a) Case 1, straight volcano. (b) Case 2, convex volcano. (c) Case 3, concave volcano. The arrows mark the boundary through which the dilute pyroclastic density current enters the computational domain, which represents the zone near the crater where the flow starts moving, aside from how it is generated (eruptive column collapse or lava dome explosion).

companion wake region [*Woods et al.*, 2002]. PDCs often move over uneven stratovolcanoes, whose shape may locally change the above mentioned behavior, and make predicting flow evolution and deposition quite challenging. This is the reason why a computational analysis on how the volcano shape affects the boundary layer processes is done in this paper.

3. Multiphase Processes Over Stratovolcanoes: A Numerical Model

[14] Numerical simulations are here performed on a two-dimensional (2-D) computational domain with three different base geometries, which mimic a straight (case 1, Figure 2a), a convex (case 2, Figure 2b), and a concave (case 3, Figure 2c) stratovolcano. The domain is 5 km long and 1.9 km high, whereas the volcano has a height of 1.5 km, comparable to that of Vesuvius (Italy) or Soufrière Hills volcano (Montserrat).

[15] A 200 m thick PDC, which is modeled as a mixture of a dusty gas and discrete particles, is simulated moving over the three geometries in order to highlight the effects of the volcano shape. The dusty gas is turbulent, compressible,, and multispecies, and it is composed of a mixture of volcanic gas, which is in thermomechanical equilibrium with a 0.1% volumetric concentration of fine ash, and atmospheric air. The equations solved for the dusty gas are the balance equations for mass, momentum, energy, species, and turbulence.

[16] Three grain-size classes of particles, 1, 5, and 10 mm, are simulated for the discrete phase by solving the equation of particle motion. The particles are two-way coupled with the dusty gas, which means that they are tracked on the basis of fluid solution and they affect, at the same time, fluid momentum, turbulence, and energy.

[17] The model is implemented ad hoc for simulating PDCs that flow over stratovolcanoes by using the Fluent 6.3 software package of computational fluid dynamics [*Fluent Inc.*, 2006].

3.1. Fluid Phase

[18] The bulk properties of the current are defined by the dusty gas approximation, wherein very fine particles and volcanic gas are assumed to be in thermal and mechanical equilibrium.

[19] The dusty gas is characterized by the following properties [*Marble*, 1970]: density $\alpha = (1 + m_s)\rho_g$, kinematic viscosity $\beta = \mu_g/\alpha$, and specific heats at both constant pressure and volume $\gamma_{p,v} = (c_{pg,vg} + m_s c_s)/(1 + m_s)$, which are modified with respect to the pure volcanic gas to account for

the very fine particles. ρ_g, μ_g, c_{pg}, and c_{vg} are density, molecular viscosity, and specific heats at constant pressure and volume of the volcanic gas, respectively. m_s and c_s are mass concentration and specific heat of the very fine particles, respectively.

[20] The turbulent behavior of the PDC is modeled by the Reynolds averaged Navier–Stokes (RANS) approach to the mixture of the dusty gas and atmospheric air. The fluid dynamic variables of the turbulent flow may have significant variations over short time scales so they have to be treated statistically. A "placeholder" variable ψ (representing dusty gas-air mixture velocity u, thermodynamic pressure p, dusty gas-air mixture density ρ, dusty gas-air mixture temperature T, and its derived quantities), in a specific time t, is given by the sum of a time-averaged part $\bar{\psi}$ and a fluctuating part ψ', $\psi = \bar{\psi} + \psi'$. The overbar indicates the time-averaging procedure over a time interval that is large compared with the period of the random fluctuations associated with turbulence, but small with respect to the nonrandom variations of the unsteady flow field. In this paper, since the dusty gas-air mixture is compressible, the mass-weighted (or Favre) averaging model is convenient. The generic variable ψ is defined as $\psi = \tilde{\psi} + \psi''$, where $\tilde{\psi} = \overline{\rho\psi}/\bar{\rho}$ is the mass-averaged part and ψ'' is the new fluctuating part. It is important to note that only the velocity components and thermal variables are mass averaged.

[21] The governing equations for modeling the dusty gas-air mixture of the PDC are the mass-averaged, two-dimensional, unsteady, compressible, equations for mass, momentum, and energy conservation, or Navier–Stokes equations. In tensor notation (the subscripts i, j, and k vary from 1 to 2) and Cartesian coordinates, the equations are

$$\frac{\partial \bar{\rho}}{\partial t} + \frac{\partial}{\partial x_j}\left(\bar{\rho}\tilde{u}_j\right) = 0, \tag{1}$$

$$\frac{\partial}{\partial t}\left(\bar{\rho}\tilde{u}_i\right) + \frac{\partial}{\partial x_j}\left(\bar{\rho}\tilde{u}_i\tilde{u}_j - \tilde{\tau}_{ij}^{\mathrm{tot}}\right) + \frac{\partial \bar{p}}{\partial x_i} - \bar{\rho}g_i = 0, \tag{2}$$

$$\frac{\partial}{\partial t}\left(\bar{\rho}\tilde{E}\right) + \frac{\partial}{\partial x_j}\left(\bar{\rho}\tilde{u}_j\tilde{E} + \tilde{u}_j\bar{p} + \tilde{q}_j^{\mathrm{tot}} - \tilde{u}_i\tilde{\tau}_j^{\mathrm{tot}}\right) = 0, \tag{3}$$

respectively, where x is a spatial coordinate, g is gravity acceleration (it acts only in vertical direction),

$$\tilde{E} = \tilde{e} + \frac{\tilde{u}_i\tilde{u}_i}{2} + k \tag{4}$$

is the total energy per unit mass; $\tilde{e}$ is the internal energy per unit mass and

$$k = \frac{\overline{u_i'' u_i''}}{2} \tag{5}$$

is the turbulent kinetic energy. The total stress tensor $\tilde{\tau}_{ij}^{\mathrm{tot}} = \tilde{\tau}_{ij}^{\mathrm{lam}} + \tilde{\tau}_{ij}^{\mathrm{turb}}$ is the sum of the viscous stress tensor

$$\tilde{\tau}_{ij}^{\mathrm{lam}} = \mu\left[\left(\frac{\partial \tilde{u}_i}{\partial x_j} + \frac{\partial \tilde{u}_j}{\partial x_i}\right) - \frac{2}{3}\delta_{ij}\frac{\partial \tilde{u}_k}{\partial x_k}\right] \tag{6}$$

and the Reynolds stress tensor, which can be related to the average velocity field through the Boussinesq hypothesis:

$$\tilde{\tau}_{ij}^{\mathrm{turb}} = -\overline{\rho u_i'' u_j''} \approx \mu_t\left[\left(\frac{\partial \tilde{u}_i}{\partial x_j} + \frac{\partial \tilde{u}_j}{\partial x_i}\right) - \frac{2}{3}\delta_{ij}\frac{\partial \tilde{u}_k}{\partial x_k}\right] - \frac{2}{3}\bar{\rho}k\delta_{ij}, \tag{7}$$

where μ is the dusty gas-air mixture molecular viscosity, δ_{ij} is the Kronecker delta ($\delta_{ij} = 1$ if $i = j$ and $\delta_{ij} = 0$ if $i \neq j$), and μ_t is turbulent viscosity.

[22] Turbulent viscosity is modeled as follows:

$$\mu_t = \bar{\rho}C_\mu\frac{k^2}{\varepsilon}, \tag{8}$$

where C_μ is an empirical constant equal to 0.0845 [*Fluent Inc.*, 2006] and ε is the turbulent dissipation rate. A two-equation turbulence model is used for modeling the unknown μ_t, the renormalization group (RNG) k-ε model, which adds the following equations for k and ε:

$$\frac{\partial}{\partial t}\left(\bar{\rho}k\right) + \frac{\partial}{\partial x_j}\left(\bar{\rho}\tilde{u}_j k\right) = \frac{\partial}{\partial x_j}\left[\alpha_k(\mu + \mu_t)\frac{\partial k}{\partial x_j}\right] + \tilde{\tau}_{ij}^{\mathrm{turb}}\frac{\partial \tilde{u}_i}{\partial x_j} - \bar{\rho}\varepsilon - \frac{\mu_t}{\bar{\rho}\mathrm{Pr}_t}g_i\frac{\partial \bar{\rho}}{\partial x_j} - 2\bar{\rho}\varepsilon\frac{kc_v}{R\tilde{T}c_p}, \tag{9}$$

$$\frac{\partial}{\partial t}\left(\bar{\rho}\varepsilon\right) + \frac{\partial}{\partial x_j}\left(\bar{\rho}\tilde{u}_j\varepsilon\right) = \frac{\partial}{\partial x_j}\left[\alpha_\varepsilon(\mu + \mu_t)\frac{\partial \varepsilon}{\partial x_j}\right] + C_{1\varepsilon}\frac{\varepsilon}{k}\tilde{\tau}_{ij}^{\mathrm{turb}}\frac{\partial \tilde{u}_i}{\partial x_j} - C_{2\varepsilon}\bar{\rho}\frac{\varepsilon^2}{k} - R_\varepsilon, \tag{10}$$

where

$$R_\varepsilon = \frac{C_\mu\bar{\rho}\eta^3(1 - \eta/4.38)}{1 + 0.012\eta^3}\frac{\varepsilon^2}{k} \tag{11}$$

is a term that accounts for the large deformation rates of the dusty gas-air mixture occurring in the zones of the domain where the PDC interacts with the different volcano shapes. The empirical constants α_k, α_ε, $C_{1\varepsilon}$, and $C_{2\varepsilon}$ are equal to 1.393, 1.393, 1.42, and 1.68, respectively [*Fluent Inc.*, 2006]. The mean strain rate tensor $\tilde{S}_{ij}$ is accounted for in η through $\tilde{S}$ by the following equations:

$$\eta \equiv \tilde{S}k/\varepsilon, \tag{12}$$

$$\tilde{S} = \left(2\tilde{S}_{ij}\tilde{S}_{ij}\right)^{1/2}, \tag{13}$$

$$\tilde{S}_{ij} = \frac{1}{2}\left(\frac{\partial \tilde{u}_i}{\partial x_j} + \frac{\partial \tilde{u}_j}{\partial x_i}\right). \tag{14}$$

The total heat flux $\tilde{q}_j^{\mathrm{tot}}$ is defined by Fourier's law and is given by

$$\tilde{q}_j^{\mathrm{tot}} = -c_p\left(\frac{\mu}{\mathrm{Pr}} + \frac{\mu_t}{\mathrm{Pr}_t}\right)\frac{\partial \tilde{T}}{\partial x_j}, \tag{15}$$

where Pr and Pr_t are the laminar and turbulent Prandtl numbers, respectively, and c_p is the dusty gas-air mixture specific heat at constant pressure.

[23] The dusty gas-air mixture is treated as an ideal gas with the following equation of state:

$$\bar{p} = \bar{\rho} R \tilde{T} \sum_n \left(\frac{Y_n}{M_n} \right), \tag{16}$$

where R is the universal gas constant, Y_n is the mass fraction of the nth species (dusty gas and air), and M_n is the molecular weight of the nth species. The following state equation is used for relating internal energy per unit mass to temperature:

$$\tilde{e} = c_v \tilde{T}, \tag{17}$$

where c_v is the dusty gas-air mixture's specific heat at constant volume.

[24] The last two terms on the right-hand side of equation (9) account for the effects of buoyancy on an ideal gas and compressibility or dilatation (or dissipation) on the dusty gas-air mixture turbulence, respectively.

[25] The dusty gas-air mixture density, molecular viscosity, and specific heats are calculated by volume-weighted and mass-weighted mixing laws (mixture of dusty gas and atmospheric air). The continuity equation for the conservation of the dusty gas and atmospheric air is given by

$$\frac{\partial}{\partial t}(\bar{\rho} Y_n) + \frac{\partial}{\partial x_j}\left(\bar{\rho} \tilde{u}_j Y_n\right) = -\frac{\partial}{\partial x_j}(J_n), \tag{18}$$

where

$$J_n = -\left(\bar{\rho} D_n + \frac{\mu_t}{Sc_t} \right) \frac{\partial}{\partial x_j}(Y_n) \tag{19}$$

is the mass diffusion flux of the nth species, which is defined by the Fickian diffusion law for dilute flows and accounts for molecular and turbulent diffusions of the dusty gas into the air. D_n is the molecular diffusion coefficient of the nth species and Sc_t is the turbulent Schmidt number. One equation for each species is implemented for multispecies models, but in this case only that for the dusty gas is solved since $n = 2$ and $\sum_n Y_n = 1$ is always true.

3.2. Particles

[26] The Euler-Lagrange approach has been recently used to model the transport capacity of PDCs and substrate-flow interaction [*Doronzo*, 2011, 2012; *Doronzo and Dellino*, 2011; *Doronzo et al.*, 2010, 2011; *Valentine et al.*, 2011]. In this paper, the calculation of the Lagrangian particle trajectories is made by means of the balance of forces acting on the discrete phase within the dusty gas-air mixture.

[27] The theoretical limit of this approach is that the volumetric concentration of the discrete phase in each computational cell could not exceed 10%–12% [*Fluent Inc.*, 2006]. This is due to the strongly nonlinear coupling between particle and gas phases at such high concentrations, which is better modeled using a multifield approach [*Valentine and Wohletz*, 1989; *Dartevelle*, 2004]. However, using the dusty gas approach reduces the difference between the mass concentration of the discrete phase and the dusty gas-air mixture. This is an important point in favor of the dusty gas-Lagrange combined approach with two-way coupling, which thus also allows simulating the particle motion in which the concentration exceeds the above mentioned limit. Details on the dusty gas-Lagrange method are found in the work by *Doronzo et al.* [2010].

[28] The Lagrangian particle trajectories are calculated by solving the equation of motion for realistically shaped particles. The balance between body (inertial) forces of a particle and surface forces acting on the particle, per unit particle mass, can be written, in the i direction, as

$$\frac{d\tilde{u}_{i,p}}{dt} = F_{D,i}\left(\tilde{u}_i - \tilde{u}_{i,p}\right) + \frac{g_i\left(\rho_p - \bar{\rho}\right)}{\rho_p}, \tag{20}$$

where

$$F_{D,i} = \frac{18\mu}{\rho_p {d_p}^2} \frac{C_D Re_r}{24}, \tag{21}$$

$$Re_r = \frac{\bar{\rho} d_p |\tilde{u}_{i,p} - \tilde{u}_i|}{\mu}, \tag{22}$$

$\tilde{u}_p$ is the particle velocity, ρ_p is the particle density, d_p is the particle diameter, and C_D is the particle drag coefficient. The term $g_i(\rho_p - \bar{\rho})/\rho_p$ accounts for gravity acceleration in the vertical direction; it is zero in the horizontal direction. To account for the real shape of volcanic particles, the C_D value is calculated as follows [*Dellino et al.*, 2005];

$$C_D = \frac{0.69 g_i {d_p}^3 \bar{\rho}\left(1.33\rho_p - 1.33\bar{\rho}\right)}{\mu^2 \left(\frac{g_i \phi^{1.6} {d_p}^3 \bar{\rho}\left(\rho_p - \bar{\rho}\right)}{\mu^2} \right)^{1.0412}}, \tag{23}$$

where φ is the particle shape parameter that is set to 0.6, which is reasonable for moderately vesicular pyroclasts [*Dellino et al.*, 2005]. It is worth noting that the particle trajectories are predicted by using the average velocity of the dusty gas-air mixture, $\tilde{u}$, in equation (20).

[29] Particles, especially the finer ones, can be subject to turbulent dispersion caused by the fluctuating part of fluid velocity. A stochastic tracking model [*Fluent Inc.*, 2006] is used to account for this effect, so the Lagrangian particle trajectories are predicted by using the instantaneous velocity of the dusty gas-air mixture, $\tilde{u} + u''$. The fluctuating part, u'', is calculated by solving the equation for turbulent kinetic energy k and assuming it is isotropic,

$$\sqrt{\overline{u_i''^2}} = \sqrt{\frac{2}{3}k} \tag{24}$$

and characterizing the turbulent eddies with a Gaussian probability distribution. In this way, u_i'' is given by

$$u_i'' = \xi \sqrt{\overline{u_i''^2}}, \tag{25}$$

where ξ is a normally distributed random number. The trajectories are calculated for a relatively great number of

particles to guarantee the statistically random effect of turbulence on particle dispersion.

[30] Finally, a simple heat balance is used to relate particle temperature $\tilde{T}_p$ to the convective heat transfer that is due to the Lagrangian particles:

$$m_p cc_p \frac{d\tilde{T}_p}{dt} = \sigma A_p \left(\tilde{T} - \tilde{T}_p\right), \tag{26}$$

where m_p is the particle mass, cc_p is the particle specific heat, σ is the convective heat transfer coefficient of the particle, and A_p is the particle surface area.

3.3. Fluid-Particle Interaction

[31] An important concept in the analysis of multiphase flows is the "coupling" between different phases, which describes the exchange of mass, momentum, and energy in the actual thermomechanical condition of the multiphase system [*Balachandar and Eaton*, 2010]. When the phases are perfectly coupled, as in dusty gases, no exchanges occur, whereas decoupled phases do exchange the conservative quantities among each other. When the mass concentration of the phases is comparable, the coupling is said to be "two-way" and accounts for the reciprocal effect of a phase on another.

[32] Two-way coupling by momentum transfers between the dusty gas-air mixture and a solid phase is accounted for in this paper and consists of introducing an additional term in the momentum equation of the dusty gas-air mixture on its left-hand side (equation (2)). This term expresses the momentum transfer from the dusty gas-air mixture to the solid phase and is computed by examining the momentum changes of the particles as they pass through the computational cells. It depends on the aerodynamic resistance characteristics of the particles and is given by

$$-\frac{1}{\Omega}\sum_f F_{D,i}^f \left(\tilde{u}_{i,p} - \tilde{u}_i\right)\dot{m}_p \Delta t, \tag{27}$$

which is an interchange force integrated over the cell surface per unit of dusty gas-air mixture volume Ω. The particle mass flow rate $\dot{m}_p$ is evaluated through faces f of each cell, and Δt is the integration time step. The momentum transfer from the solid phase to the dusty gas-air mixture is accounted for by the first term on the right-hand side of equation (20). The two-way coupling implementation for momentum is very important because it allows turbulence modulation, i.e., the effect of particles on the dusty gas-air mixture turbulence, and turbulent dispersion, i.e., the effect of the dusty gas-air mixture turbulence on the particles.

[33] Two-way coupling by energy transfers between the dusty gas-air mixture and solid phase is also accounted for, which consists of introducing an additional term in the energy equation of the dusty gas-air mixture on its left-hand side (equation (3)). This term expresses the energy transfer from the dusty gas-air mixture to the solid phase and is computed by examining the energy changes of the particles as they pass through the computational cells. It is given by

$$-\frac{1}{\Omega}\left(cc_p \Delta\tilde{T}_p \dot{m}_p\right), \tag{28}$$

where $\Delta\tilde{T}_p$ is the change of Lagrangian particle temperature in the cells. The energy transfer from the solid phase to the dusty gas-air mixture is accounted for by the right-hand side of equation (26). The two-way coupling for energy is important in considering the effect of the Lagrangian particle concentration on dusty gas-air mixture compressibility.

3.4. Particle-Substrate Interaction

[34] Particle saltation is allowed when the particles touch the ground. Particles are subject to saltation and not to direct deposition (stopping) because they strike the ground surface with different impact angles. According to *Dufek et al.* [2009], the interaction of the Lagrangian particles with the wall is defined by slightly anelastic rebound, which is a function of the impact angle; for simplicity, a constant restitution coefficient for particle momentum of 0.85 is used. The particles most prone to deposition are the ones that rebound perpendicularly, reflecting a complete loss of tangential momentum.

3.5. Numerical Technique

[35] The set of equations is solved numerically with a cell-centered finite-volume method, using Ansys Fluent software [*Fluent Inc.*, 2006]. All the equations are integrated over the computational cells (75,000, each 3–8.5 m along slope, and 0.2 m vertical) and time step (0.1 s), so each term is discretized, and the involved dependent variables are allocated at the cell centers in time. The system of equations can be referred to as a classic computational fluid dynamics problem of convection-diffusion-dominated flows and represents the transport equations for the variables.

[36] The convection terms are discretized by an implicit second-order upwind-differencing scheme and the diffusion terms by an implicit second order central-differencing scheme. The transient terms are discretized by an implicit three-time-level scheme, i.e., an implicit second-order backward-differencing scheme. The pressure gradient is discretized by a linear interpolation scheme.

[37] The discretized set of equations is implemented by the implicit "segregated" method, which means that for a given dependent variable, the unknown value is computed at each cell center by interpolating the same unknown from the adjacent cell centers. In this way, each variable appears in more than one equation (one/cell) at each time level so the equations are solved separately for each variable (segregated) but simultaneously (implicit) for all the cells.

[38] An iterative method is used to solve the system of equations, which consists of guessing a solution for an independent variable and solving for the value of the associated dependent variable while keeping the other dependent variables fixed. A point-implicit (Gauss-Seidel) method is coupled with an algebraic multigrid method for improving the solution guesses by an iterative procedure, which is necessary because the discretization scheme is implicit and because of the nonlinearity of the equations.

[39] The accuracy of the solution is guaranteed by the second-order discretization of both the spatial and temporal terms. The stability of the solution is ensured by the implicit method, which is unconditionally stable and not limited by stability constraints. The trend of errors for each equation is monitored during calculation and sometimes is reduced by means of the underrelaxation techniques. The convergence of

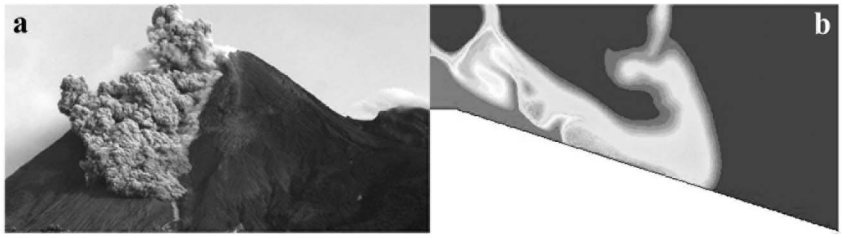

Figure 3. Dilute pyroclastic density currents generated during unidirectional eruptions start as a homogeneous flow, and then are subject to stratification of velocity and density because of the no-slip condition and atmospheric air friction, and particle sedimentation, respectively. (a) Unidirectional explosion occurred during the recent eruption of Mount Merapi (Indonesia) in late 2010. (b) Simulation of the initially homogeneous dilute pyroclastic density current that moves over the straight stratovolcano (case 1), with the gray scale representing the dusty gas mass fraction (toward the black area is air only). The comparison of flow evolution between Figures 3a and 3b, from homogeneous to stratified, is only qualitative but this kind of evolution is experienced by any particle-laden turbulent currents.

the solution is controlled by checking that the residuals decrease to lower than 10^{-3} for each equation.

4. Computational Runs

[40] The computational runs work as follows: At the initial instant, a hot (573 K) mixture of pure dusty gas, i.e., with no air, and volumetric 1% of each particle enters the domain with a velocity of 20 m/s, constant with height, and then it mixes with a initially static standard atmosphere. The feeding for the mixture is kept constant over minutes (3.3 to 7.5 min, depending on geometry) in order to provide a quasi-steady flow condition, which is used for the calculations on the simulated PDC. Also, the initial particle concentration is relatively low (3%), and the total number of Lagrangian particles used in the simulations depends on grid resolution and run duration, which means that 3.4×10^5, 5.4×10^5, and 2.4×10^5 particles/particle size are calculated for case 1, case 2, and case 3, respectively.

[41] The initial flow is of a wall type, i.e., the volcanic (column or dome) collapse is not simulated and starts at the instant when the PDC starts moving, aside from how it is generated (valid for all mechanisms; Figure 3). It starts with a small forced convection in order to allow monitoring the aerodynamic effects of the stratovolcanoes on the flow behavior. This justifies the relatively low momentum (product of flow density and velocity) of the initial PDC. The mixture first moves over a horizontal distance of 100 m; then it starts interacting with the different geometries. This distance is enough to allow the turbulent boundary layer development before the interaction occurs in order to have a PDC that approaches the geometries as a stratified flow. The average slope angle was set at about 17° for all three geometries. In this way, the role of volcano aerodynamics on particle behavior at sedimentation can be better highlighted since the slope angle does not overcome particle respose angle.

5. Results

[42] Profiles of flow velocity are calculated from the simulations, and they are shown in Figures 4, 5, and 6 at direct distances of 100, 1000, 2000, 3000, and 4000 m from the inlet of the domain (collapse zone). The velocities are calculated at the time when the head of the flow is at the foot of the volcano and the body, continuously fed upstream, is quasi steady. The PDC is on average 50 m thick, which is thinner than it is at the start because of the relatively steep slopes it encounters, so the velocity profiles are 50 m high. It is chosen to monitor the velocity in order to relate the depositional processes to the boundary layer structure. This would result in predicting numerically the style of deposition from a PDC based on the velocity profile, or vice versa, in constraining the flow behavior based on the PDC deposits.

[43] The approach used for calculating the profiles benefits from the results of *Valentine et al.* [2011], who have simulated numerically the deposition over stratovolcanoes by measuring the sediment flux toward the substrate (particle mass flow rate per unit surface) as a function of volcano shape. Here, the analysis of boundary layer evolution as a function of the three shapes of stratovolcanoes is made by postprocessing those results, showing the flow velocity, and interpreting the profiles in light of the multiphase boundary layer characteristics and the sediment flux data.

[44] The difference of the two approaches, sediment flux versus boundary layer based and particle versus fluid flow based, stands in the way of postprocessing data and showing results, respectively. This paper is based on the idea that the fluid phase of a PDC is not only the transport system for the particles but is also the depositional system, which means that the deposition itself can be predicted on the basis of flow velocity (toward zero velocity is deposition).

5.1. Velocity Profiles

[45] The profile at 100 m (Figures 4–6) shows that the turbulent boundary layer is just developed, whereas the wake region is not formed yet, which means that close to the crater the no-slip condition acts more rapidly than air friction in establishing the flow structure. This allows the flow to exacerbate the velocity gradient in the lower part and to maintain a nearly homogeneous velocity in the upper part, which causes an en masse particle feeding to the substrate [*Branney and Kokelaar*, 2002] and hence the emplacement of thick massive deposits through a high sediment flux [*Valentine et al.*, 2011].

[46] As the PDC travels, the boundary layer thickens and the wake region develops, and the rate of growth depends on the ground shape over which the fluid flow moves. Massive

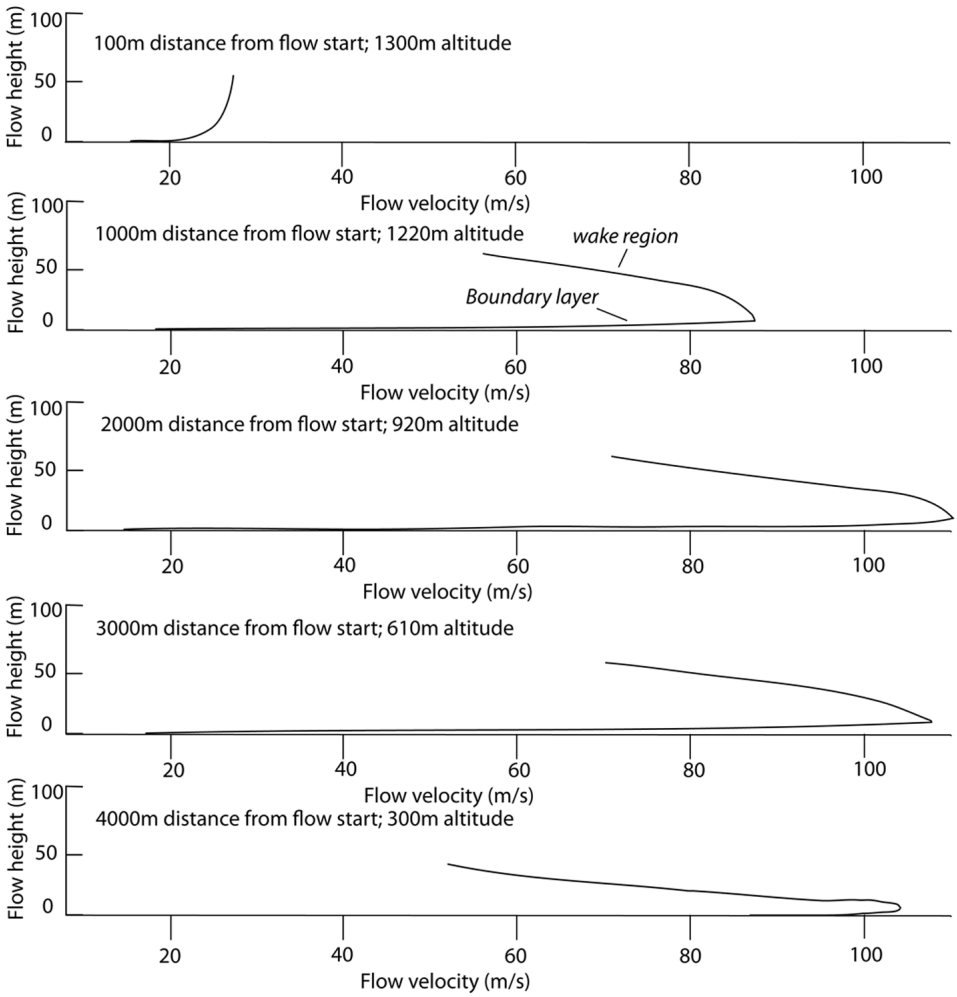

Figure 4. Velocity profiles of the dilute pyroclastic density current calculated at direct distances of 100, 1000, 2000, 3000, and 4000 m from the vent for case 1 (straight stratovolcano). The boundary layer is represented by the lower, increasing upward velocity, whereas the wake region is represented by the upper, decreasing upward velocity.

deposits are always generated in proximal areas (≤1 km from crater) for the three cases, but their total thickness, as well as that of each depositional unit (sum of units is total deposit), i.e., the layer, strongly varies based on the stratovolcano shape. The layers look thicker for case 2 (Figure 5) than for case 1 (Figure 4), and particularly case 3 (Figure 6) because the boundary layer is relatively thinner and the wake region is less pronounced. The deposition occurs layer-by-layer, since once the particle load is emplaced, it acts as new substrate for the flow. In distal areas (≥3 km from crater), both the boundary layer and the wake region are fully developed in all three cases (Figures 4, 5, and 6). This causes a progressive particle feeding to the substrate [*Branney and Kokelaar*, 2002] and hence the emplacement of thin laminated deposits through a low sediment flux [*Valentine et al.*, 2011], which are likely capped by massive deposits of fine ash resulting from slow settling from the wake region when the flow wanes. The boundary layer thickness is nearly the same for the three cases; in fact the laminated deposit thickness is similar [*Valentine et al.*, 2011] and therefore the lamina thickness is also expected to be similar. The deposition is lamina-by-lamina, i.e., the total deposit is the sum of laminae aggradation, because the boundary layer reacts more rapidly to the process of lamina formation than it does during the layer-by-layer deposition. The reaction time is directly proportional to the thickness of the flow boundary zone, which is the basal part of the lower flow where the sedimentary structures are acquired [*Branney and Kokelaar*, 2002]. A calculation of the boundary layer reaction time and depositional unit thickness is provided in the following discussion for the convex stratovolcano (case 2) as representative of two extreme depositional styles (layer forming and lamina forming) described for the PDC. The choice of case 2 for the calculation lies in the evidence of a more dramatic evolution of the boundary layer over the convex shape (Figure 5).

[47] The thickness of the fine-ash deposits likely varies as a function of the stratovolcano shape since it occurs as particle-by-particle sedimentation from the wake region [*Dellino et al.*, 2010b], which is quite different for the three cases. These deposits are expected to be thicker for case 3 (Figure 6) than for case 1 (Figure 4), and particularly case 2 (Figure 5), because the upper velocity profile is concave upward, which

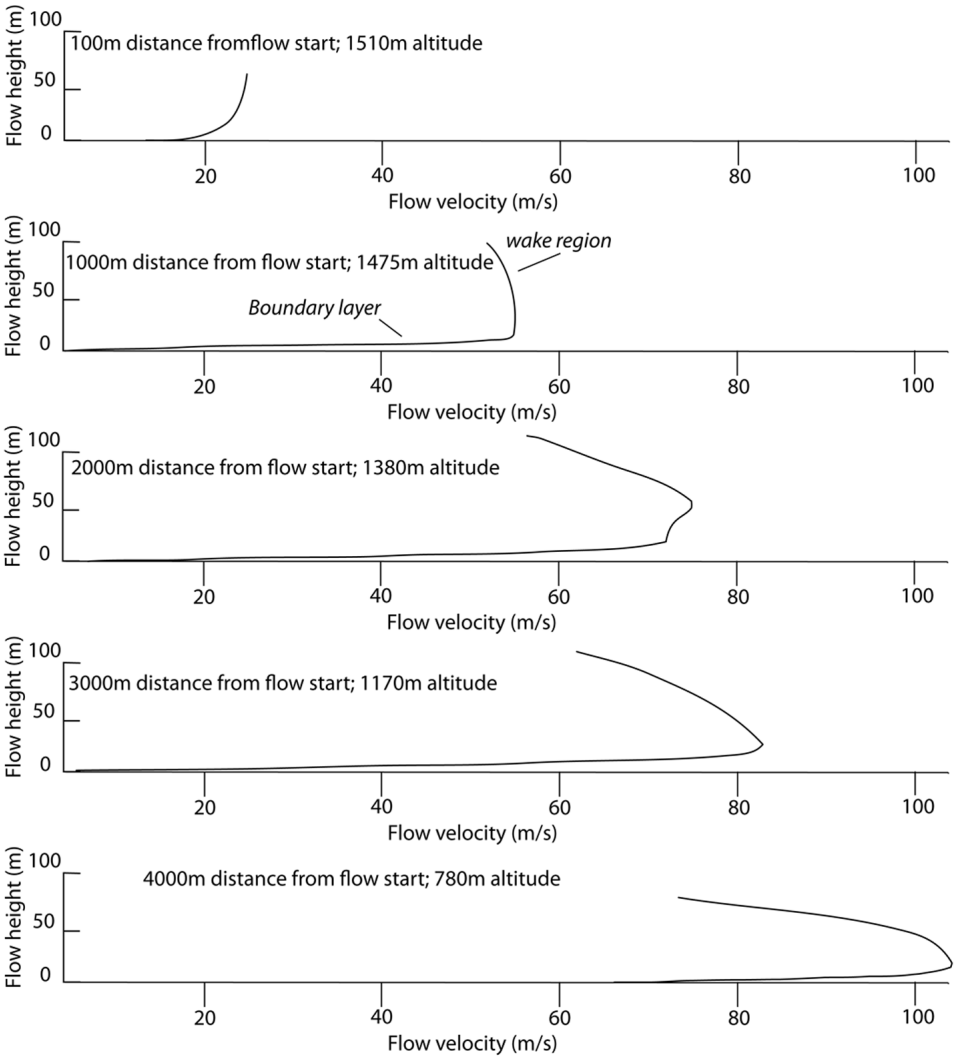

Figure 5. Velocity profiles of the dilute pyroclastic density current calculated at direct distances of 100, 1000, 2000, 3000, and 4000 m from the vent for case 2 (convex stratovolcano). The boundary layer is represented by the lower, increasing upward velocity, whereas the wake region is represented by the upper, decreasing upward velocity.

means that a lot of fine ash may first loft because of strong turbulence [*Hoffmann et al.*, 1985; *Muck et al.*, 1985; *Valentine et al.*, 2011], and then it may gently settle after the laminated deposits are emplaced. This late particle-by-particle deposition is hypothesized here on the basis of postprocessing and is not directly simulated (much longer computational runs are needed), so it would need to be better constrained by ad hoc simulations and experiments. Anyway, field evidences show that a break in slope (concave upward type) may produce high lofting of fine ash, which gently settles and overlays the stratified deposits [*Saucedo et al.*, 2004; *Sulpizio et al.*, 2007; *Doronzo and Dellino*, 2010], confirming our hypothesis. This probably means that higher lofting, and hence turbulence, leads to thicker, fine-ash facies, at the top PDC deposits. The shape of the wake region profile follows the volcano geometry, i.e., it is convex for convex stratovolcanoes (Figure 5), concave for concave stratovolcanoes (Figure 6), and straight for geometries in between (Figure 4). The fine-ash deposits probably form not only in distal areas, but always where the wake region is quite developed, so they are also expected in the medial area (2 km from crater) for case 2 (Figure 5) and proximal-to-medial areas for cases 1 and 3 (Figures 4 and 6).

5.2. Calculation of Boundary Layer Reaction Time and Depositional Unit Thickness

[48] Some concepts of the sediment mechanics on turbidity currents [*Allen*, 1991; *Doronzo and Dellino*, 2010] are used here to calculate the boundary layer reaction time and depositional unit thickness. An application of the calculations is done for the convex stratovolcano (case 2, Figure 2b) in proximal (1 km from crater) and distal (4 km from crater) areas, since this is the case in which a more dramatic evolution of the boundary layer occurs (Figure 5). The two calculations, proximal and distal, could be considered as end-members of boundary layer processes and depositional styles.

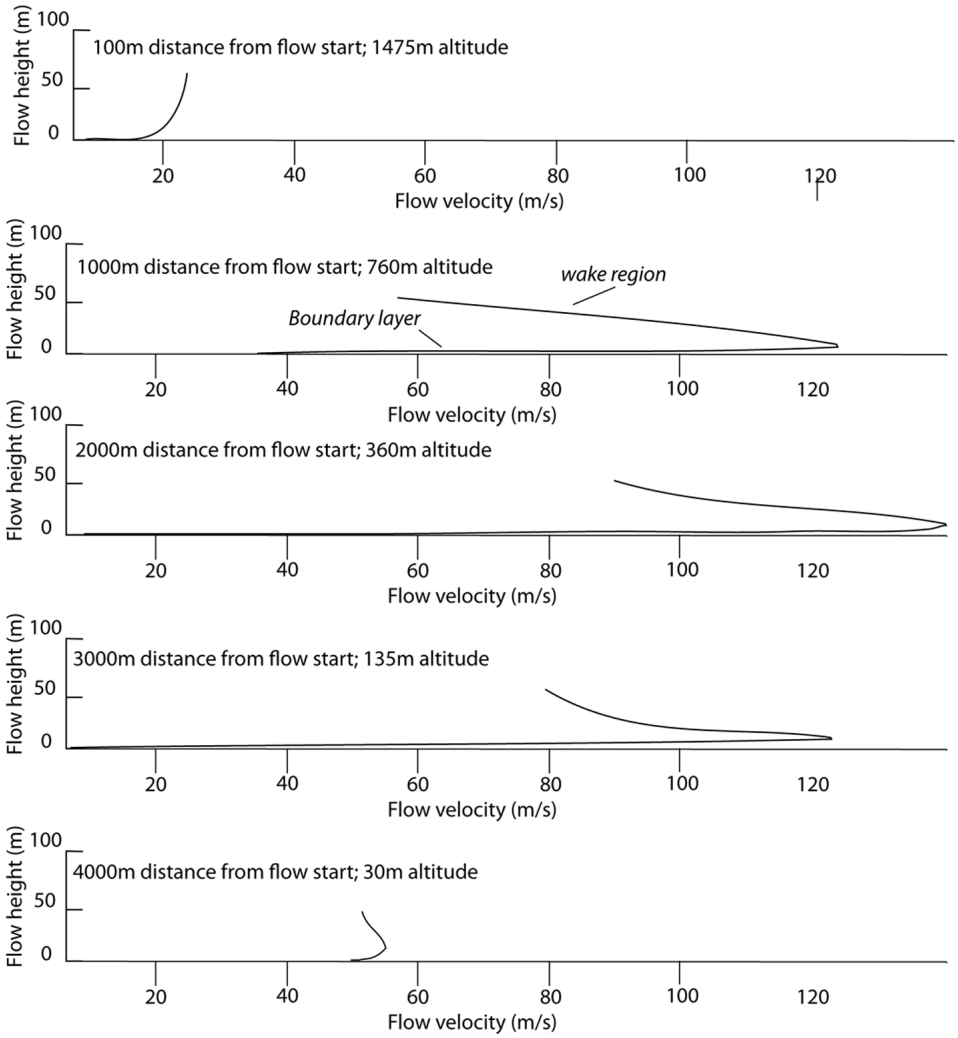

Figure 6. Velocity profiles of the dilute pyroclastic density current calculated at direct distances of 100, 1000, 2000, 3000, and 4000 m from the vent for case 3 (concave stratovolcano). The boundary layer is represented by the lower, increasing upward velocity, whereas the wake region is represented by the upper, decreasing upward velocity.

[49] Some concepts developed for turbidity currents can be applied to PDCs on the basis of their fluid dynamic similarity [*Doronzo and Dellino*, 2010] when a few vol % of sand-grained particles represent the solid load for the flow [*Allen*, 1991; *Kubo*, 2004]. A limitation of the similarity is that the flow of PDCs is compressible, whereas that of turbidity currents is generally not, but this would not affect its application to dilute PDCs when the regime is depositional and flow velocity is well under sound speed (slight compressibility). For a quasi-steady flow, such as that simulated for PDCs when they reach the foot of the volcano, the upward velocity of deposit growth, v, is given by

$$v = \frac{h}{t}, \tag{29}$$

and it is assumed constant in the formation time t of deposit of h thickness. This velocity is the same for each depositional unit (layer or lamina) forming the whole deposit. The time of depositional unit formation t_u and therefore the boundary layer reaction time is given by

$$t_u = \frac{h_u}{v}, \tag{30}$$

where h_u is the depositional unit thickness, which is approximated by [*Doronzo and Dellino*, 2010]

$$h_u = H\bar{C} \tag{31}$$

by assuming that deposition occurs by progressive aggradation perpendicular to the substrate [*Middleton and Southard*, 1984]. H is the flow thickness, and $\bar{C}$ is the average particle concentration, which is given by

$$\bar{C} = \frac{1}{H}\int_0^H C(y)dy, \tag{32}$$

where $C(y)$ is the particle concentration as a function of height y. In equation (31), H tends to overestimate h_u, whereas $\bar{C}$ tends to underestimate it, but this effect tends to be balanced in currents with moderate to good sorting. In the proximal area, h is equal to 13.78 m and t is equal to 450 s [*Valentine et al.*, 2011], which gives a value for v of 0.03 m/s. H and $\bar{C}$ are calculated from the simulation, and they are equal to 54 m and 0.11, respectively, which gives a value for h_u of 5.94 m. The resulting value for t_u thus is 198 s. The same calculations are done in the distal area, with values for h and t of 0.17 m and 450 s, respectively [*Valentine et al.*, 2011], and result in a value for v of 0.0004 m/s. The results of H and $\bar{C}$ are 50 m and 0.0002, respectively, and they give a value for h_u of 0.01 m. The resulting value for t_u is 25 s.

[50] By analyzing the calculated values of the boundary layer reaction time t_u and depositional unit thickness h_u, some considerations on deposit characteristics can be done. Thick deposits of metric (at most about 6 m) massive layers are generated in the proximal area, whereas thin mill metric laminated deposits (at most 10 mm) form in the distal area. The proximal deposits are emplaced from a boundary layer not fully developed, which has a time of the order of minutes (at least 3 min) to react to the particle deposition process. The distal deposits are emplaced from a boundary layer at its maximum development, and the reaction time is of the order of several seconds (at most 25 s). This means that lamination is suppressed in the proximal area because of a high sediment flux toward the substrate, which is what also happens in sandy turbidity currents when the velocity of deposit growth is in excess of 0.0007 m/s [*Arnott and Hand*, 1989; *Allen*, 1991]. Our calculation suggest that finely laminated deposits form in the distal area with a growth velocity of about half a millimeter per second, which agrees quite well with the turbidity literature (lamination is favored when $v < 0.0007$ m/s).

[51] Where the turbulent boundary layer is not fully developed (proximal area), the average particle concentration is higher than where it is fully developed (distal area), and a higher sediment flux is expected through a thicker flow boundary zone [*Valentine et al.*, 2011]. Particles, both the coarser and the finer ones [*Valentine et al.*, 2011], cannot thus be moved by traction (which favors the formation of deposit lamination by shear movement) over a sharp flow-substrate boundary zone [*Kneller and Branney*, 1995] because the high downward sediment flux encumbers traction [*Allen*, 1991; *Giordano and Dobran*, 1994]. Therefore, a better sorting of particles, confirmed by some natural deposits of turbidity currents [*Gladstone and Sparks*, 2002] and PDCs [*Branney and Kokelaar*, 2002], occurs at the flow base where particle concentration is lower. Also, good sorting occurs at the flow top where fine particles migrate from the Kelvin-Helmholtz vortices, which thicken as the flow dilutes (toward the distal area), as a function of particle inertia [*Cantero et al.*, 2008].

6. Example From the 1997 Boxing Day Volcanic Blast on Montserrat

[52] Most of the numerical simulations of explosive eruptions make use of the multifield approach (Euler-Euler formulation), which treats the solid phase (particles) as a continuum [e.g., *Valentine et al.*, 1992; *Clarke et al.*, 2002; *Dufek and Bergantz*, 2007; *Esposti Ongaro et al.*, 2008]. The approach used in this paper follows an Euler-Lagrange formulation, and it allows the estimation of deposition from PDCs by focusing on the boundary layer processes. These two approaches can have mutual benefits in characterizing the dynamics of the current and the depositional process of PDCs of actual volcanoes when used in combination. An example is provided by the 1997 Boxing Day volcanic blast on Montserrat, West Indies, in which the multifield approach has allowed calculating the PDC velocity profiles in different locations of the island [*Esposti Ongaro et al.*, 2008]. In the 2-D simulations of the blast, the PDC moves over the actual topographic profile, which can be approximated by case 1 (Figure 2a) of our simulations, since it has dimensions and conformation similar to those of our straight stratovolcano. In the work by *Esposti Ongaro et al.* [2008], results are shown at a distance of 3.4 km from the PDC source area and can be compared to the profiles calculated at 3 and 4 km for our simulated case 1. In both cases, a boundary layer and a fully developed wake region, which is probably indicative of lamina-by-lamina deposition, are detectable in the simulation results. Additionally, field evidences [*Druitt et al.*, 2002] show laminated deposits from a dilute PDC cropping out in the same zone where *Esposti Ongaro et al.* [2008] have calculated the velocities.

[53] The comparison between the simulations of this paper and the ones of *Esposti Ongaro et al.* [2008], supported by the field evidences of *Druitt et al.* [2002], makes us confident that our method is in line with the actual knowledge of PDCs in volcanology and can contribute to better constraining the link between flow behavior and deposition from density currents.

7. Conclusions

[54] The three geometries adopted for simulating stratovolcanoes affected by PDC inundation represent simple end-members of volcano shapes. In nature, straight- or concave-like stratovolcanoes are more common than convex-like ones, the latter being generally represented by shield volcanoes, but sometimes they show some sectors (near-crater zone or distal morphological high) of the edifice with different shapes, so an uneven stratovolcano may be comprehensive of all three cases. Moreover, the topography that surrounds a stratovolcano is often involved in the propagation of PDCs, and this further complicates the shape of the volcanic complex.

[55] The facies of deposits generated by a PDC is frequently reported in the literature as showing a proximal-to-distal (massive versus stratified) lateral transition, together with vertical facies variations [e.g., *Branney and Kokelaar*, 2002]. This is in agreement with the results of our simulation. Furthermore, our simulations are based on a technique that is already validated by large-scale experiments [*Doronzo et al.*, 2011].

[56] Besides a general agreement with the evidences of PDC deposit described in the literature, our simulations show that a strong relationship exists between the boundary layer conditions and the formation of deposits. They tend to be thick or thin, massive or laminated, depending on the boundary layer thickness. They can be capped by fine-ash deposits, whose thickness depends on the shape of the wake

region. Thin boundary layers would produce thick deposits of massive layers, whereas thick boundary layers would produce thin laminated deposits. Concave wake regions would produce thick deposits of fine ash, whereas convex wake regions would produce thin deposits of fine ash. Moreover, a continuum spectrum of facies variations exists in between, for example, the formation of relatively thick laminated deposits generated by relatively thick boundary layers.

[57] It is worth concluding that the quantitative analysis presented here is based on two assumptions: (1) the current is quasi steady, which is reasonable in our case since in the simulations velocities changed by less than 1.2 m/s after 420. This may not always be the case in natural PDCs, especially for short-lived currents (v changes in time) [*Branney and Kokelaar*, 2002; *Sulpizio and Dellino*, 2008]. (2) The deposition is by progressive aggradation perpendicular to the substrate. This may not always occur in nature, especially where PDCs move over uneven topographies [*Branney and Kokelaar*, 2002; *Sulpizio and Dellino*, 2008]. Anyway, these limitations do not preclude the use of our results as a tentative guideline for interpreting deposit features as functions of volcano shape and flow behavior. They can serve for predicting the style of deposition from a PDC based on the velocity profile or, vice versa, for predicting the flow behavior based on the PDC deposit facies architecture.

[58] **Acknowledgments.** Two anonymous reviewers are thanked for helping to improve the manuscript. D. M. Doronzo also thanks G. A. Valentine for discussions on stratovolcanism.

References

Allen, J. R. L. (1991), The Bouma division A and the possible duration of turbidity currents, *J. Sediment. Petrol.*, *61*, 291–295.

Arnott, R. W. C., and B. M. Hand (1989), Bedforms, primary structures and grain fabric in the presence of sediment rain, *J. Sediment. Petrol.*, *59*, 1062–1069.

Balachandar, S., and J. K. Eaton (2010), Turbulent dispersed multiphase flow, *Annu. Rev. Fluid Mech.*, *42*, 111–133, doi:10.1146/annurev.fluid.010908.165243.

Branney, M. J., and P. Kokelaar (1992), A reappraisal of ignimbrite emplacement: Progressive aggradation and changes from particulate to non-particulate flow during emplacement of high-grade ignimbrite, *Bull. Volcanol.*, *54*, 504–520, doi:10.1007/BF00301396.

Branney, M. J., and P. Kokelaar (2002), Pyroclastic density currents and the sedimentation of ignimbrites, *Mem. 27*, Geol. Soc., London.

Burgisser, A., and G. W. Bergantz (2002), Reconciling pyroclastic flow and surge: The multiphase physics of pyroclastic density currents, *Earth Planet. Sci. Lett.*, *202*, 405–418, doi:10.1016/S0012-821X(02)00789-6.

Bursik, M., and A. W. Woods (1996), The dynamics and thermodynamics of large ash flows, *Bull. Volcanol.*, *58*, 175–193, doi:10.1007/s004450050134.

Cantero, M. I., M. H. Garcia, and S. Balachandar (2008), Effect of particle inertia on the dynamics of depositional particulate density currents, *Comput. Geosci.*, *34*, 1307–1318, doi:10.1016/j.cageo.2008.02.002.

Cas, R. A. F., and J. V. Wright (1987), *Volcanic Successions: Modern and Ancient*, Allen and Unwin, London, doi:10.1007/978-94-009-3167-1.

Clarke, A. B., B. Voight, A. Neri, and G. Macedonio (2002), Transient dynamics of vulcanian explosions and column collapse, *Nature*, *415*, 897–901, doi:10.1038/415897a.

Dartevelle, S. (2004), Numerical modeling of geophysical granular flows: 1. A comprehensive approach to granular rheologies and geophysical multiphase flows, *Geochem. Geophys. Geosyst.*, *5*, Q08003, doi:10.1029/2003GC000636.

Dellino, P., R. Isaia, and M. Veneruso (2004), Turbulent boundary layer shear flow as an approximation of base surge at Campi Flegrei, *J. Volcanol. Geotherm. Res.*, *133*, 211–228, doi:10.1016/S0377-0273(03)00399-8.

Dellino, P., D. Mele, R. Bonasia, G. Braia, L. La Volpe, and R. Sulpizio (2005), The analysis of the influence of pumice shape on its terminal velocity, *Geophys. Res. Lett.*, *32*, L21306, doi:10.1029/2005GL023954.

Dellino, P., D. Mele, R. Sulpizio, L. La Volpe, and G. Braia (2008), A method for the calculation of the impact parameters of dilute pyroclastic density currents based on deposits particle characteristics, *J. Geophys. Res.*, *113*, B07206, doi:10.1029/2007JB005365.

Dellino, P., et al. (2010a), Conduit flow experiments help constraining the regime of explosive eruptions, *J. Geophys. Res.*, *115*, B04204, doi:10.1029/2009JB006781.

Dellino, P., R. Buttner, F. Dioguardi, D. M. Doronzo, L. La Volpe, D. Mele, I. Sonder, R. Sulpizio, and B. Zimanowski (2010b), Experimental evidence links volcanic particle characteristics to pyroclastic flow hazard, *Earth Planet. Sci. Lett.*, *295*, 314–320, doi:10.1016/j.epsl.2010.04.022.

Doronzo, D. M. (2010), Could the Twin Towers collapse teach the interaction between dilute pyroclastic density currents and buildings?, *Nat. Hazards*, *55*, 177–179, doi:10.1007/s11069-010-9544-3.

Doronzo, D. M. (2011), A theoretical–experimental-numerical integrated approach to pyroclastic density currents, PhD thesis, Univ. of Bari, Bari, Italy.

Doronzo, D. M. (2012), Integrating computer simulations and experiments to study explosive volcanic eruptions, *Nat. Hazards*, *60*, 785–788, doi:10.1007/s11069-011-0020-5.

Doronzo, D. M., and P. Dellino (2010), A fluid dynamic model of volcaniclastic turbidity currents based on the similarity with the lower part of dilute pyroclastic density currents: Evaluation of the ash dispersal from ash turbidites, *J. Volcanol. Geotherm. Res.*, *191*, 193–204, doi:10.1016/j.jvolgeores.2010.01.017.

Doronzo, D. M., and P. Dellino (2011), Interaction between pyroclastic density currents and buildings: Numerical simulation and first experiments, *Earth Planet. Sci. Lett.*, *310*, 286–292, doi:10.1016/j.epsl.2011.08.017.

Doronzo, D. M., G. A. Valentine, P. Dellino, and M. D. de Tullio (2010), Numerical analysis of the effect of topography on deposition from dilute pyroclastic density currents, *Earth Planet. Sci. Lett.*, *300*, 164–173, doi:10.1016/j.epsl.2010.10.003.

Doronzo, D. M., M. D. de Tullio, P. Dellino, and G. Pascazio (2011), Numerical simulation of pyroclastic density currents using locally refined Cartesian grids, *Comput. Fluids*, *44*, 56–67, doi:10.1016/j.compfluid.2010.12.006.

Druitt, T., E. S. Calder, P. D. Cole, R. P. Hoblitt, S. C. Loughlin, G. E. Norton, L. J. Ritchie, R. S. J. Sparks, and B. Voight (2002), Small-volume, highly mobile pyroclastic flows formed by rapid sedimentation from pyroclastic surges at Soufrière Hills Volcano, Montserrat: An important volcanic hazard, in *The Eruption of Soufrière Hills Volcano, Montserrat, From 1995 to 1999*, edited by T. Druitt and B. P. Kokelaar, *Geol. Soc. London, Mem. 21*, 263–279.

Dufek, J., and G. W. Bergantz (2007), Suspended-load and bed-load transport of particle-laden gravity currents: The role of particle-bed interaction, *Theor. Comput. Fluid Dyn.*, *21*, 119–145, doi:10.1007/s00162-007-0041-6.

Dufek, J., J. Wexler, and M. Manga (2009), Transport capacity of pyroclastic density currents: Experiments and models of substrate-flow interaction, *J. Geophys. Res.*, *114*, B11203, doi:10.1029/2008JB006216.

Esposti Ongaro, T., A. Clarke, A. Neri, B. Voight, and C. Widiwijayanti (2008), Fluid-dynamics of the 1997 Boxing Day lateral blast of Soufrière Hills volcano (Montserrat, WI), *J. Geophys. Res.*, *113*, B03211, doi:10.1029/2006JB004898.

Fluent Inc. (2006), Fluent 6.3 Manual 2006, Lebanon, N. H.

Giordano, G., and F. Dobran (1994), Computer simulations of the Tuscolano Artemisio's second pyroclastic flow unit (Alban Hills, Latium, Italy), *J. Volcanol. Geotherm. Res.*, *61*, 69–94, doi:10.1016/0377-0273(94)00013-1.

Gladstone, C., and R. S. J. Sparks (2002), The significance of grain-size breaks in turbidites and pyroclastic density current deposits, *J. Sediment. Res.*, *72*, 182–191, doi:10.1306/041801720182.

Hoffmann, P., K. Muck, and P. Bradshaw (1985), The effect of concave surface curvature on turbulent boundary layers, *J. Fluid Mech.*, *161*, 371–403, doi:10.1017/S0022112085002981.

Kneller, B. C., and M. J. Branney (1995), Sustained high density turbidity currents and the deposition of thick massive sands, *Sedimentology*, *42*, 607–616, doi:10.1111/j.1365-3091.1995.tb00395.x.

Kneller, B., S. J. Bennett, and W. D. McCaffrey (1999), Velocity structure, turbulence and fluid stresses in experimental gravity currents, *J. Geophys. Res.*, *104*, 5381–5391, doi:10.1029/1998JC900077.

Kubo, Y. (2004), Experimental and numerical study of topographic effects on deposition from two-dimensional, particle-driven density currents, *Sediment. Geol.*, *164*, 311–326, doi:10.1016/j.sedgeo.2003.11.002.

Lipman, P. W., and D. R. Mullineaux (1981), The 1980 eruption of Mount St. Helens, Washington, *U.S. Geol. Surv. Prof. Pap.*, *1250*.

Marble, F. E. (1970), Dynamics of dusty gases, *Annu. Rev. Fluid Mech.*, *2*, 397–446, doi:10.1146/annurev.fl.02.010170.002145.

Martí, J., A. Folch, G. Macedonio, and A. Neri (2000), Pressure evolution during caldera forming eruptions, *Earth Planet. Sci. Lett.*, *175*, 275–287, doi:10.1016/S0012-821X(99)00296-4.

Middleton, G. V., and J. B. Southard (1984), Mechanics of sediment movement, Soc. of Econ. Paleont. and Mineral., Tulsa, Okla.

Muck, K., P. Hoffmann, and P. Bradshaw (1985), The effect of convex surface curvature on turbulent boundary layers, *J. Fluid Mech.*, *161*, 347–369, doi:10.1017/S002211208500297X.

Saucedo, R., J. L. Macias, and M. Bursik (2004), Pyroclastic flow deposits of the 1991 eruption of Volcan de Colima, Mexico, *Bull. Volcanol.*, *66*, 291–306, doi:10.1007/s00445-003-0311-0.

Sulpizio, R., and P. Dellino (2008), Sedimentology, depositional mechanisms and pulsating behaviour of pyroclastic density currents, in *Calderas Volcanism: Analysis, Modelling and Response*, vol. 10, *Developments in Volcanology*, edited by J. Marti and J. Gottsman, pp. 57–96, Elsevier, Amsterdam, doi:10.1016/S1871-644X(07)00002-2.

Sulpizio, R., D. Mele, P. Dellino, and L. La Volpe (2007), High variability of sedimentology and physical properties of pyroclastic density currents during complex Subplinian eruptions: The example of the AD 472 (Pollena) eruption of Somma-Vesuvius, Italy, *Sedimentology*, *54*, 607–635, doi:10.1111/j.1365-3091.2006.00852.x.

Sulpizio, R., R. Bonasia, P. Dellino, D. Mele, M. A. Di Vito, and L. La Volpe (2010), The Pomici di Avellino eruption of Somma-Vesuvius (3.9 ka BP). Part II: Sedimentology and physical volcanology of pyroclastic density current deposits, *Bull. Volcanol.*, *72*, 559–577, doi:10.1007/s00445-009-0340-4.

Valentine, G. A. (1987), Stratified flow in pyroclastic surge, *Bull. Volcanol.*, *49*, 616–630, doi:10.1007/BF01079967.

Valentine, G. A., and R. V. Fisher (1993), Glowing avalanches: New research on volcanic density currents, *Science*, *259*, 1130–1131, doi:10.1126/science.259.5098.1130.

Valentine, G. A., and K. H. Wohletz (1989), Numerical models of Plinian eruptions columns and pyroclastic flows, *J. Geophys. Res.*, *94*, 1867–1887, doi:10.1029/JB094iB02p01867.

Valentine, G. A., K. H. Wohletz, and S. W. Kieffer (1992), Effects of topography on facies and compositional zonation in caldera-related ignimbrites, *Geol. Soc. Am. Bull.*, *104*, 154–165, doi:10.1130/0016-7606(1992)104<0154:EOTOFA>2.3.CO;2.

Valentine, G. A., D. M. Doronzo, P. Dellino, and M. D. de Tullio (2011), Effects of volcano shape on dilute pyroclastic density currents: Numerical simulations, *Geology*, *39*, 947–950, doi:10.1130/G31936.1.

Vazquez, A., and M. Ort (2006), Facies variation of eruption units produced by the passage of single pyroclastic surge currents, Hopi Buttes volcanic field, USA, *J. Volcanol. Geotherm. Res.*, *154*, 222–236, doi:10.1016/j.jvolgeores.2006.01.003.

Wilson, L., R. S. J. Sparks, and G. P. L. Walker (1980), Explosive volcanic eruptions–IV. The control of magma properties and conduit geometry on eruption column behaviour, *Geophys. J. R. Astron. Soc.*, *63*, 117–148.

Woods, A. W., R. S. J. Sparks, L. J. Ritchie, J. Batey, C. Gladstone, and M. I. Bursik (2002), The explosive decompression of a pressurized volcanic dome: The 26 December 1997 collapse and explosion of Soufrière Hills Volcano, Montserrat, in *The Eruption of Soufrière Hills Volcano, Montserrat, From 1995 to 1999*, edited by T. Druitt and B. P. Kokelaar, *Geol. Soc. London, Mem. 21*, 457–465.

P. Dellino and R. Sulpizio, Centro Interdipartimentale di Ricerca sul Rischio Sismico e Vulcanico, Dipartimento di Scienze della Terra e Geoambientali, Università degli Studi di Bari, Via E. Orabona 4, I-70125 Bari, Italy.

D. M. Doronzo, School of Earth and Atmospheric Sciences, Georgia Institute of Technology, 311 Ferst Dr., Atlanta, GA 30332, USA. (domenico.doronzo@eas.gatech.edu)

J. Martí, Institute of Earth Sciences "Jaume Almera," CSIC, Lluis Solé Sabaris s/n, E-08028 Barcelona, Spain.